The use of multiscale transfer functions for understanding the impact of successive mechanical treatments on surface topography

Julie Marteau, Christophe Paulin, Maxence Bigerelle

The use of multiscale transfer functions for understanding the impact of successive mechanical treatments on surface topography

Julie Marteau[a,*], Christophe Paulin[c], Maxence Bigerelle[b]

[a] *Galileo Galilei, Sorbonne Universités, Université de Technologie de Compiègne, Laboratoire Roberval, UMR-CNRS 7337, Centre de Recherches de Royallieu, 60203 Compiègne, France*
[b] *Laboratoire d'Automatique, de Mécanique et d'Informatique industrielles et Humaines LAMIH UMR-CNRS 8201, Université de Valenciennes et du Hainaut Cambrésis, Le Mont Houy, 59313 Valenciennes Cedex 9, France*
[c] *Industrial Partner, France*

ARTICLE INFO

Keywords:
Polishing
Topography
Roughness
Fractal

ABSTRACT

This paper shows how a multiscale transfer function can be used to understand the impact of successive mechanical treatments (superfinishing, sandblasting and brushing) on topography. The multiscale analysis indicates that the changes of roughness induced by brushing are not uniform on the entire range of frequencies. The transfer function built with the arithmetic mean deviation (S_a) leads to identify two regimes of roughness: the ability of brushing to "create roughness" and the ability of brushing to "remove roughness" caused by blasting.

1. Introduction

Topography conditions several key properties of surface: mechanical and tribological properties (e.g. wear resistance [1], adhesion [2], hardness [3]), chemical properties (e.g. corrosion [4]), optical properties (e.g. gloss [5]), thermal properties [6], electrical properties [7], ... Different strategies have been developed in order to link the topography with the surface functionality or the process conditions. As an example, Li et al. [8] described the relation between surface roughness and burnishing force using the assumption of Winkler foundation. Bigerelle et al. [9] used a fractal function combined with a stochastic wear model in order to model superfinishing by belt grinding process. El-Sonbaty et al. [10] developed artificial neural networks models in order to link the cutting conditions of milling and the obtained surface roughness profiles.

However, a combination of different processes (e.g. polishing, sandblasting, superfinishing, electro-discharge machining ...) is often used in order to obtain the final surface functionality of a given mechanical component. After each process, the mechanical properties and topography of the surface are modified. The issue is then to understand how each step, or more precisely each process, modifies the topography in order to be able to optimize the final surface functionality. As indicated by Thomas et al. [11], this could be named 'traceology': this is the search of a link between the changes of topography and the steps used to produce the surface.

The transfer function of the topography, defined as the ratio between the output signal and the input signal, has already been chosen as a tool for estimating surface quality but the signals used for the investigation differ from authors to authors. Hafiz et al. [12] examined the influence of overlapping between two successive laser beam tracks on surface quality using transfer functions based on the power spectral density function computed in the spatial frequency domain. Zahouani et al. [13] used three-dimensional continuous wavelet transform in order to determine the multiscale transfer function of machining by abrasion for each step of the finishing process. Wieland et al. [14] chose to characterize surface treatments composed of several processes with a transfer function defined using individual Fast Fourier Transformation coefficients. They defined multiplicative transfer functions using sets of Fast Fourier Transformation coefficients and proposed the use of additive transfer terms when the examined process tend to create new roughness components.

This paper shows how the definition of a multiscale function based on a simple roughness parameter can help understanding how the interactions between successive surface treatments lead to get the aimed surface state. This methodology of investigation is applied to a set of surfaces that were successively superfinished, sandblasted and brushed in order to get a specific brightness for watch dials. In a previous work [15], the link between roughness and brightness was searched using different roughness parameters and filtering conditions.

* Corresponding author.
E-mail address: julie.marteau@utc.fr (J. Marteau).

The best relation between roughness and brightness was identified using the arithmetic mean deviation S_a with a high-pass filter having a cut-off length of 15 µm. As using the arithmetic mean deviation S_a was found to be the most relevant roughness parameter for the examination of brightness, this paper is mainly focused on the changes of this roughness parameter, from which a multiscale transfer function is built. Section 2 of this paper is devoted to the description of the material, process parameters and roughness measurements. Section 3 investigates the effects of successive processes (superfinishing, blasting and brushing) on the topography using multiscale decomposition. These results are then discussed and conclusions are drawn.

2. Materials and methods

2.1. Material and process parameters

The examined material is brass. In order to analyze roughness changes induced by the successive processes, the topography obtained with different combinations of processes are examined:

- superfinishing alone is examined. It corresponds to the use of a finer grit solid abrasive to remove the thin surface layer produced by the initial grinding. Superfinishing is considered as the initial surface condition (there are 3 samples to examine reproducibility).
- superfinishing followed by sandblasting (there are 9 samples as different sandblasting conditions are tested),
- superfinishing followed by brushing. Brushing, also called dull polished metal, corresponds to a unidirectional satin finish (there are 3 samples to examine reproducibility),
- superfinishing, sandblasting and brushing (9 samples).

For superfinishing and brushing, the same process parameters are used on all the specimens. As for sandblasting, the nozzle-to-specimen height and pressure are varied while the nozzle angle and duration are kept constant. Nine specimens having different topographies are obtained by combining five pressure values and five nozzle-to-specimen height values. These combinations were chosen to vary the brightness of watch dials. Table 1 shows the different combinations with the corresponding specimen numbers.

2.2. Roughness measurements and multiscale analysis

For the measurement of topography, an optical profiler (WYKO NT9300, VEECO, United States) with a x100 objective is used. The measured areas have a surface of 127 µm x 92 µm, with a lateral resolution of 0.55 µm and a corresponding vertical accuracy approximately equal to 0.1 nm. Twenty measurements are made on each surface. The topography characteristics are analyzed using a multiscale decomposition of roughness with different types of filters:

- Robust Gaussian filters [16]: high-pass, low-pass and band-pass. The cut-off lengths (i.e. the wavelengths from which the filter starts filtering) are chosen in order to follow a geometric progression. There are equal to: 0.8, 1, 1.2, 1.4, 1.7, 2, 2.6, 3.1, 3.9, 4.8, 6, 7.5, 10, 13, 17, 24, 40, 60 and 120 µm. As for the band-pass filter, only the first-cut-off length of the filter is indicated. The bandwidth can be found by subtracting equal this value to the next larger cut-off length. As an example, for the label 'DE 10 µm', the first cut-off length is equal to 10 µm and the bandwidth is equal to (13−10) =3 µm.
- Discrete wavelet filters with different taps: Coiflet (1−3), Symlet (1−4), Daubechies(1−5) [17],
- Modal filters [18]: high-pass and low-pass.

Table 1
Pressure and nozzle-to-specimen values for the sandblasted specimens.

Specimen number	Nozzle distance (cm)	Pressure (bar)
1	20	0.9
2	20	2.6
3	5	0.9
4	5	2.6
5	10	1.7
6	30	1.7
7	0	1.7
8	10	0.5
9	10	3

The use of these different filters makes it possible to highlight different characteristics of waviness and surface microroughness.

As the arithmetic mean deviation S_a [19] was previously shown to be the best parameter for the description of the relation between roughness and brightness [15], the following investigation is mainly focused on the changes of this roughness parameter. All the mean values and confidence intervals (standard deviations) are obtained using 100 bootstraps. Bootstrapping consists in randomly sampling the data with replacement. It allows assigning confidence intervals and more generally measures accuracy.

3. Results and discussion

3.1. Multiscale analysis of each process

The examined brass specimens are successively superfinished, sandblasted and brushed. In order to examine how those successive processes change the surface morphology, surfaces that are only superfinished are investigated first. Then, surfaces that are successively superfinished, sandblasted and brushed are studied. It should be noted that morphology is analyzed using mainly Gaussian filters to determine the characteristic lengths of the topographies given by the different processes. The other filters were tested as well but were found less relevant (their results are often not shown for the sake of brevity).

3.1.1. Superfinishing process

First, topography modifications induced by superfinishing are analyzed using roughness measurements. The arithmetic mean deviation S_a is calculated using different types of filtering. Only the results given by the Robust Gaussian filter are hereafter discussed as only this type of filter indicates characteristic lengths of the process topography. Fig. 1 shows the arithmetic mean deviation S_a as a function of the cut-off length, using a Robust Gaussian band-pass filter for the superfinished specimens. This graph shows the distribution of the S_a mean values and the associated confidence intervals. All three superfinished specimens show similar arithmetic mean deviation values. Thus, the

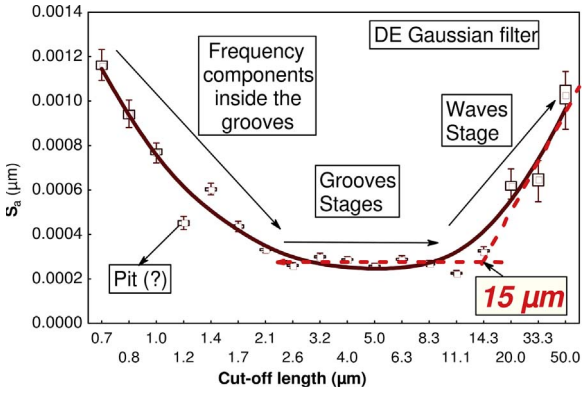

Fig. 1. Mean values and associated confidence intervals of the arithmetic mean deviation S_a as a function of the cut-off length, using a Robust Gaussian band-pass filter (DE), for the superfinished specimens.

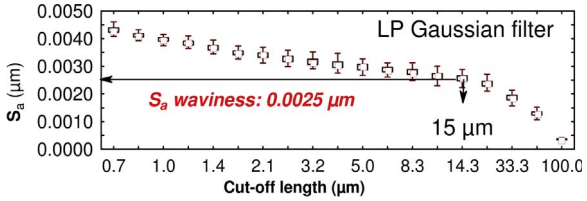

Fig. 2. Mean values and associated confidence intervals of the arithmetic mean deviation S_a as a function of the cut-off length, using a Robust Gaussian low-pass filter (LP), for the superfinished specimens.

topography induced by the superfinishing process is quite homogeneous. A finer examination of Fig. 1 leads to identify three main regimes. The first one appears for cut-off length values below 2 µm and corresponds to the fractal part. This reflects the groove dimensions. The second regime corresponds to cut-off lengths comprised between 3 µm and 10 µm. This second regime is stable and corresponds to the grooves. The third and last regime is found for cut-off lengths above 15 µm and reflects the presence of waviness, which is independent of the grooves.

In order to observe waviness, a Robust Gaussian low-pass filter with a cut-off length equal to 15 µm is used, as shown in Fig. 2. The latter shows that the waviness amplitude is equal to 0.0025 µm. To check whether the identified regime really corresponds to waviness, another roughness parameter is examined: the mean density of furrows. This parameter is based on the segmentation of the topography into small units called motifs, through the use of the watershed algorithm [20]. The frontiers of the dale motifs provide a linear description of the topography (called furrows) whose length is measured and then divided by the considered area, thus giving the mean density of furrows. Fig. 3 shows the mean density of furrows as a function of the cut-off length using a band-pass wavelet filter. The maximum value of the mean density of furrows is found for a cut-off length of 15 µm. It corresponds to the end of the appearance of grooves and thus confirms the previous results. Finally, a Robust Gaussian high-pass filter is used in order to obtain the arithmetic mean deviation of the grooves. Fig. 4 shows the arithmetic mean deviation S_a as a function of the cut-off length using a Robust Gaussian high-pass filter. Thanks to the slope change, the arithmetic mean deviation S_a of the grooves can be identified. According to this graph, it is equal to 5 nm.

Hereafter, superfinished surfaces are considered as the initial surface condition.

3.1.2. Blasting and brushing processes

After superfinishing, the samples are sandblasted using different process parameters and finally brushed. In order to observe the topography changes induced by sandblasting alone and sandblasting followed by brushing, the arithmetic mean deviation S_a is plotted as a function of the cut-off length, using a Gaussian band-pass filter (Fig. 5). A first quick glance at the graphs for the superfinished and sandblasted specimens and for the superfinished, sandblasted and brushed specimens shows that there are strong variations of S_a values: the S_a value

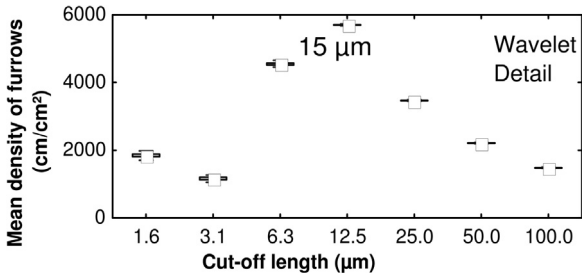

Fig. 3. Mean values and associated confidence intervals of the mean density of furrows as a function of the cut-off length using a wavelet band-pass filter, for the superfinished specimens.

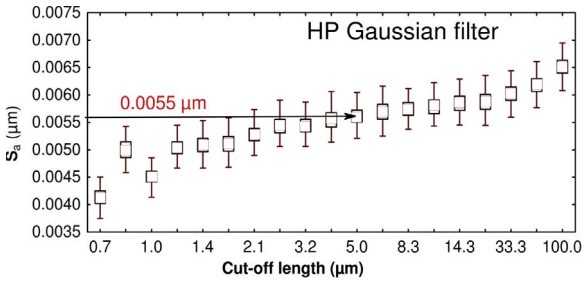

Fig. 4. Mean values and associated confidence intervals of the arithmetic mean deviation S_a as a function of the cut-off length, using a Robust Gaussian high-pass filter (HP), for the superfinished specimens.

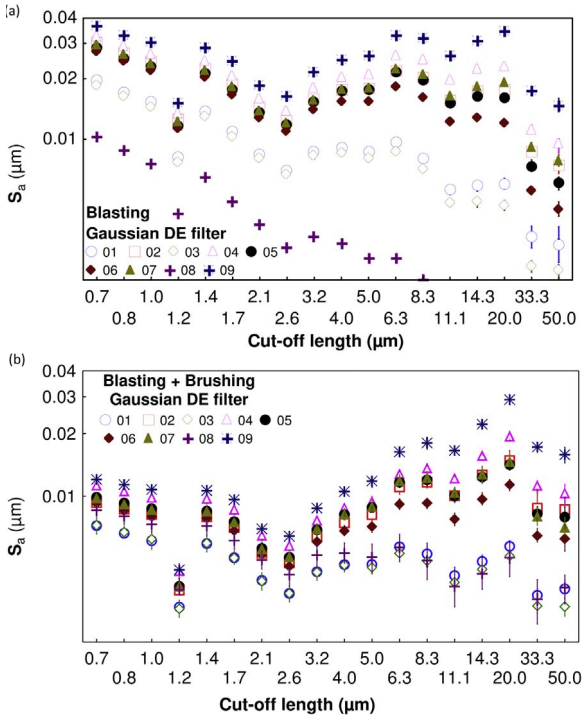

Fig. 5. The arithmetic mean deviation S_a as a function of the cut-off length, using a Robust Gaussian band-pass filter (DE), for (a) the superfinished and sandblasted specimens and (b) the superfinished, sandblasted and brushed specimens.

depends on the filtering and above all on the sample type. The addition of brushing also modifies the S_a values: this was expected but it is worth noting that changes are not homothetic. This lack of homothetic transformation means that the effects of brushing are not uniform on all the frequencies. Furthermore, this lack of homothetic transformation is different from specimen to specimen and is thus linked with the blasting conditions. Brushing transfer depends on the incoming roughness.

3.2. Transfer function using the arithmetic mean deviation S_a

By definition, a transfer function is equal to the output signal divided by the incoming signal. Thus, in this case, the transfer function is defined as the arithmetic mean deviation S_a measured on the superfinished, sandblasted and brushed specimens divided by the S_a measured on the superfinished and sandblasted specimens. The transfer function is computed for each cut-off length. Based on the transfer function values, three cases can be identified:

(i) The transfer function value is equal to unit: there are no roughness changes or more precisely, the arithmetic mean deviation does not enable us to detect any topography modifications.

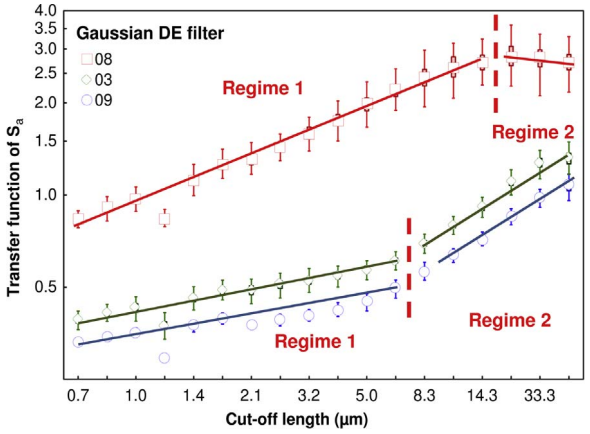

Fig. 6. Mean values and associated confidence intervals of the transfer function of the arithmetic mean deviation S_a as a function of the cut-off length using a Robust Gaussian band-pass filter. The results are given for Sample 3, 9 and 10, which show extreme values.

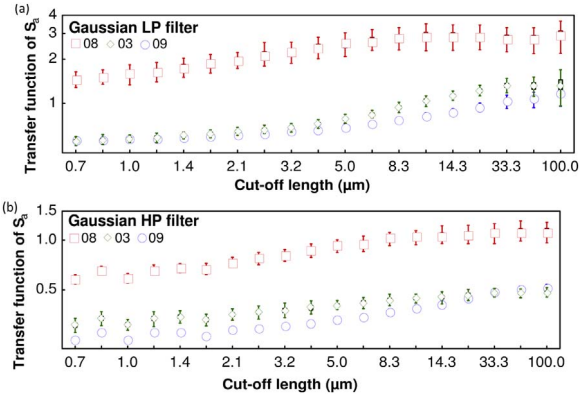

Fig. 7. Mean values and associated confidence intervals of the transfer function of the arithmetic mean deviation S_a as a function of the cut-off length using (a) a Robust Gaussian low-pass (LP) filter and (b) a Robust Gaussian high-pass (HP) filter The results are given for Sample 3, 9 and 10, which show extreme values.

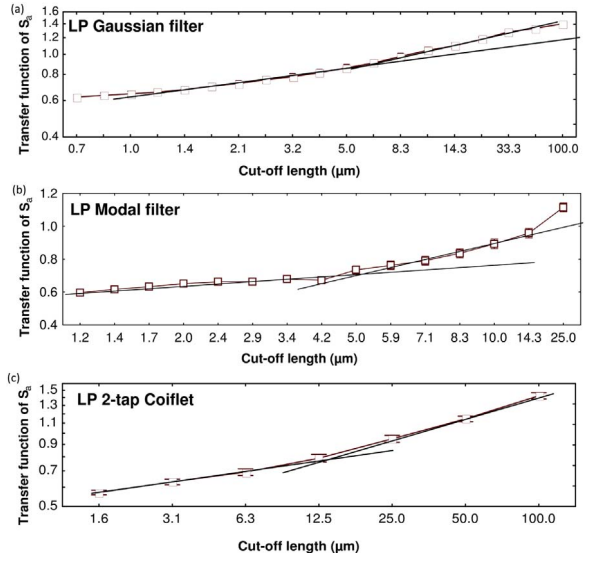

Fig. 8. Mean values and associated confidence intervals of the average transfer function of the arithmetic mean deviation S_a as a function of the cut-off length using (a) a Robust Gaussian low-pass (LP) filter and (b) a low-pass modal filter and (c) a 2-tap Coiflet filter.

(ii) The transfer function value is above unity: the brushing process increases roughness.
(iii) The transfer function value is below unity: the brushing process decreases roughness.

Fig. 6 shows the transfer function of S_a as a function of the cut-off lengths, using a Robust Gaussian band-pass filter. Only the results of Sample 3, 8 and 9 are shown as they are identified as extreme cases.

It can be observed on Fig. 6 that the values of the transfer function of S_a for Specimen 8 are mainly above unity. It means that roughness is mainly created by brushing: the sandblasting process induced very small roughness that is rapidly overcome by the topography created with brushing. For this specimen, two regimes can be identified. The first one corresponds to a linear increase of the transfer function value with the increase of the cut-off length. This indicates that practicing brushing on the morphology created with sandblasting increases roughness. Above 15 µm, a second regime is identified: there is a slight decrease but based on the confidence intervals, it can be seen as a plateau. In this second regime, roughness is only due to sandblasting. In order to better observe both regimes, the transfer function of S_a as a function of the cut-off length is plotted using a low-pass and a high-pass filter, as illustrated by Fig. 7. The use of a low-pass filter highlights the stationary state of roughness during the second regime. This is a constant waviness caused by brushing. For the first regime, a power-law can be identified. This power-law corresponds to roughness created at the scale of the grooves: it shows that roughness transfer at the scale of the grooves is not constant but is multiscale. Processes based on abrasion often give rise to multiscale structures [21].

Whatever the filtering conditions, the results of the transfer functions for Specimen 3 and 9 are different from those obtained for Specimen 8. Roughness also decreases but, during Regime 2, roughness transfer is smaller for low frequencies: the massive peaks of sandblasting are stronger with an increase of their size. The cut-off length between the regimes is approximately equal to 7 µm for both specimens but the growths are different. Specimen 9, rougher because of the blasting process, wears out more quickly in average than Specimen 3 which is smoother. It is worth noting that with the band-pass filter, there is a uniform vertical shift of the curves (with the logarithmic scale): this probably indicates a shared mechanism for the creation of roughness. The roughness of the rougher specimen is decreased more uniformly than the one of the smoother specimen. As a logarithmic scale is used in the graph, the term “uniformly” should be tempered.

It is worth noting that the previous graphs showed that the transition from Regime 1 to Regime 2 displayed little variations between specimens: the transition takes place at approximately the same scale for all the specimens. Thus, despite the use of different sandblasting parameters, there is a roughly constant transition zone that could lead to the calculation of an average transfer function for all the specimens. This average transfer function would help the understanding of the entire process and thus the analysis of the influence of the process parameters on the resulting topography. Fig. 8 displays the calculation of this average transfer function as a function of the cut-off lengths using (a) a Robust Gaussian low-pass filter and (b) a Modal low-pass filter and (c) a 2-tap Coiflet filter. Whatever the type of filter, two linear parts can be identified with the use of a logarithmic scale. This is typical for fractal multiscale processes, in which the exponent is linked with the fractal dimension. Thus, in the graphic, the slope is linked to the fractal dimension and characterizes the multiscale transfer of both treatments. The first slope corresponds to the ability to print the brushing pattern while the second slope displays the ability to remove the roughness caused by blasting. The transition zone between the regimes is neat, particularly when observed with the modal filter.

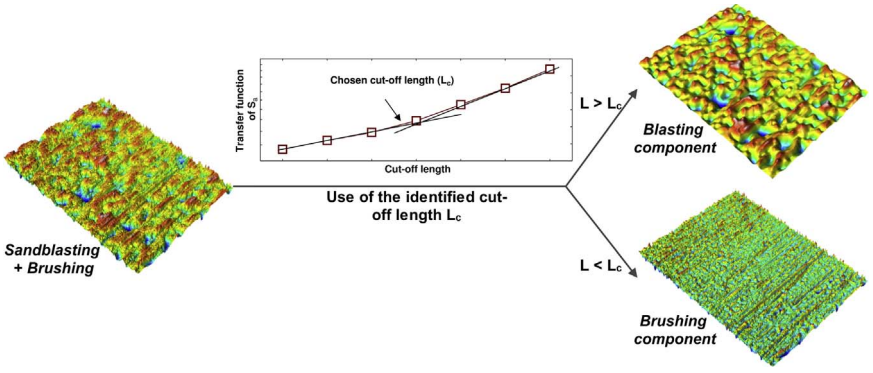

Fig. 9. Schematic summary of the methodology used for the identification of the process components.

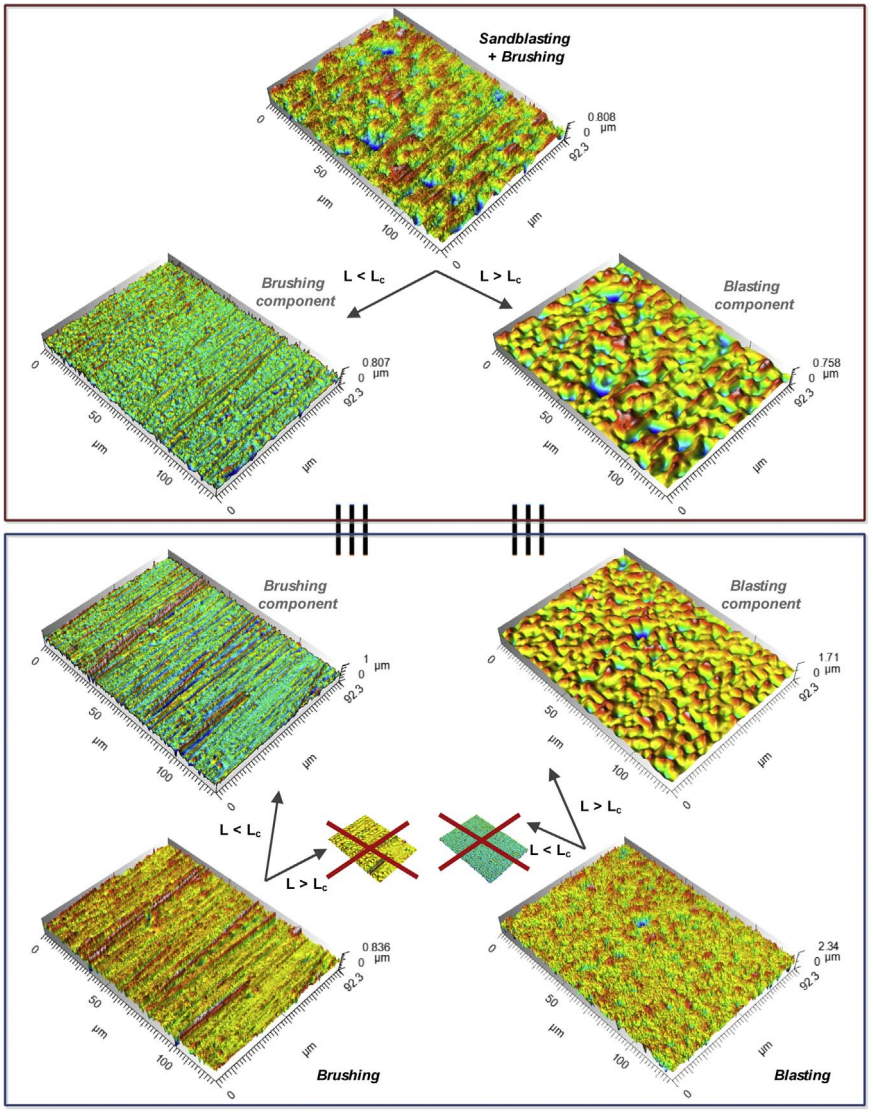

Fig. 10. Schematic summary of the elementary decomposition of the process signature.

3.3. Fractal aspect of the transfer function of S_a

The previous results can be checked using a mathematical description of the fractal aspects. Sandblasting and brushing are both fractal processes [22–25]. Thus, for each process, the arithmetic mean deviation S_a can be described using the following self-affine function [26]:

$$S_a(\varepsilon) = S_{a0}\left(\frac{\varepsilon}{\varepsilon_0}\right)^{2-H}, \tag{1}$$

where H is the Holder exponent, which is comprised between 0 and 1 and ε_0 is the gauge.

Thus, when this formula is applied to the transfer function, the following expression is obtained:

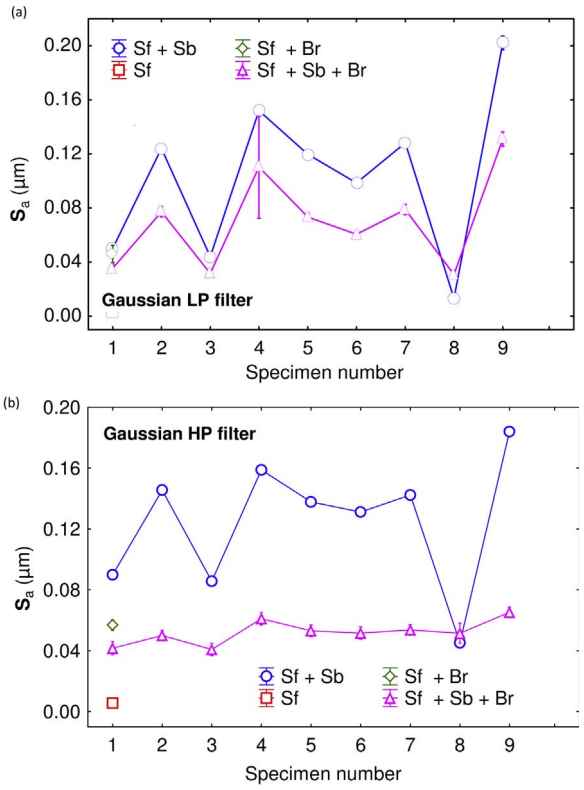

Fig. 11. Mean values and associated confidence intervals of the arithmetic mean deviation S_a using (a) a low-pass filter and (b) a high-pass filter. The cut-off length is equal to 12.5 µm. All the specimens are illustrated: Sf, Sb and Br stand for superfinishing, sandblasting and brushing respectively.

$$Tr(\varepsilon) = \frac{S_{a0_o}\left(\frac{\varepsilon}{\varepsilon_{0o}}\right)^{2-H_o}}{S_{a0_i}\left(\frac{\varepsilon}{\varepsilon_{0i}}\right)^{2-H_i}} = \frac{S_{a0_o}}{S_{a0_i}}\left(\frac{{\varepsilon_{0i}}^{2-H_i}}{{\varepsilon_{0o}}^{2-H_o}}\right)\varepsilon^{H_i-H_o}, \tag{2}$$

where index o and index i stand respectively for the output (superfinished, sandblasted and brushed) and the input (superfinished and sandblasted) of the transfer function. In Eq. (2), the term $H_i - H_o$ is comprised between −1 and 1. The slopes of Fig. 8 match this interval.

Using the previous results, the signature of the different processes can be identified by decomposing roughness. The sandblasting and brushing components can be separated from the finished surface (obtained with superfinishing, sandblasting and brushing) using the cut-off length separating the two previously identified regimes. Fig. 8(c) enables us to identify a particular cut-off length equal to 12.5 µm, which clearly separates two regimes. Below 12.5 µm, roughness transfer is controlled by brushing whereas above this value, the sandblasting component is preponderant. Thus, filtering the finished surface with a cut-off length of 12.5 µm with a coiflet filter will separate the brushing and blasting components: below 12.5 µm, the brushing component of roughness is obtained while above 12.5 µm, the sandblasting component is obtained. Fig. 9 summarizes this methodology.

3.4. Validation of the decomposition

Several hypotheses were made in order to identify the relevant cut-off length: the identified cut-off length value is independent of the process parameters and the fractal aspect of roughness and finally the discrimination was made using only one roughness parameter, which is the arithmetic mean deviation S_a. In order to validate these hypotheses, a methodology is built. To check the results, specimens that are only superfinished, and brushed are used as reference specimens: they are used to compare the surface components predicted by the transfer function from the surface components obtained for the specimens that were superfinished, sandblasted and brushed. Similarly, superfinished and sandblasted specimens are used to compare the surface components predicted by the transfer function from the surface components obtained for the specimens that were superfinished, sandblasted and brushed. The methodology philosophy is shown in Fig. 10. As indicated, the superfinished, sandblasted and brushed surfaces were filtered in order to get the sandblasting and brushing components. This morphological operation is displayed on the upper part of the figure. The obtained surfaces are compared to the surfaces corresponding to either the only brushed specimens or the ones that were only sandblasted. Both are also filtered because brushing and sandblasting interact with each other: some frequency components linked to both processes will be removed. This corresponds to the lower part of Fig. 10. It can be observed in Fig. 10 that similar textures are obtained for the blasting components and brushing components. The different filtered topographies, showing the roughness components of blasting and brushing, are fairly similar in magnitude as well as in frequency. The anisotropic component of brushing is preserved too. For the sake of brevity, the decomposition of only one specimen is shown but similar observations were made for the other specimens. These first observations show that several topographical structures are preserved despite the use of a one-frequency filtering with a model built using a simple roughness parameter: the arithmetic mean deviation S_a. Despite its simplicity, the transfer function of S_a enables us to split the mechanisms into their morphological specificities.

In order to expand these results and get quantitative information, the values of the arithmetic mean deviation S_a obtained for all the specimens (superfinished only/ superfinished and brushed/ superfinished and sandblasted/ superfinished, sandblasted and brushed) are computed using a low pass-filter and a high-pass filter with a cut-off length equal to 12.5 µm. The results are shown in Fig. 11. The low-pass filter makes it possible to observe roughness caused by sandblasting (that can be modified by brushing). Specimens 1 and 3 have similar S_a before and after brushing. In these cases, brushing does not create plateau as it does not erode the peaks. On the contrary, for Specimen 8, roughness is only created by brushing. The high-pass filter shows the roughness due to brushing and thus enables us to confirm these results: the S_a values of Specimen 8 are equal before and after brushing. For all the specimens, the S_a values diminish after brushing. Both graphs show that the decrease of the S_a values caused by brushing depends on sandblasting intensity. These observations confirm the previous results.

4. Conclusion

The arithmetic mean deviation S_a of the specimen surface depends on the filtering as well as on the examined specimen, whatever the observed treatment (superfinished and sandblasted or superfinished, sandblasted and brushed). The S_a value changes are not homothetic from sandblasted surfaces to sandblasted and brushed surfaces: this indicates that the changes made by the brushing process are not uniform on the entire range of frequencies.

The transfer function built with the arithmetic mean deviation S_a is used to identify two regimes of roughness:

(i) The ability of brushing to create roughness,
(ii) The ability of brushing to delete roughness caused by blasting.

This paper showed how the use of a multiscale transfer function can help the understanding of the topography resulting from the interaction of the different processes. Such information can then be used for the optimization of a given functionality linked to roughness, for example, in the case of this study, brightness.

References

[1] Kubiak KJ, Liskiewicz TW, Mathia TG. Surface morphology in engineering applications: influence of roughness on sliding and wear in dry fretting. Tribol Int 2011;44:1427–32.

[2] Hubert C, Marteau J, Deltombe R, Chen YM, Bigerelle M. Roughness characterization of the galling of metals. Surf Topogr: Metrol Prop 2014;2:1–9.

[3] Marteau J, Bigerelle M. Relation between surface hardening and roughness induced by ultrasonic shot peening. Tribol Int 2015;83:105–13.

[4] Ryu JJ, Shrotriya P. Influence of roughness on surface instability of medical grade cobalt–chromium alloy (CoCrMo) during contact corrosion–fatigue. Appl Surf Sci 2013;273:536–41.

[5] Briones V, Aguilera JM, Brown C. Effect of surface topography on color and gloss of chocolate samples. J Food Eng 2006;77:776–83.

[6] Cui T, Li Q, Xuan Y. Characterization and application of engineered regular rough surfaces in thermal contact resistance. Appl Therm Eng 2014;71:400–9.

[7] Ketenoğlu D, Ünal B. Influence of surface roughness on the electrical conductivity of semiconducting thin films. Phys A: Stat Mech Appl 2013;392:3008–17.

[8] Li FL, Xia W, Zhou ZY, Zhao J, Tang ZQ. Analytical prediction and experimental verification of surface roughness during the burnishing process. Int J Mach Tools Manuf 2012;62:67–75.

[9] Bigerelle M, Hagege B, El Mansori M. Mechanical modelling of micro-scale abrasion in superfinish belt grinding. Tribol Int 2008;41:992–1001.

[10] El-Sonbaty IA, Khashaba UA, Selmy AI, Ali AI. Prediction of surface roughness profiles for milled surfaces using an artificial neural network and fractal geometry approach. J Mater Process Technol 2008;200:271–8.

[11] Thomas TR, Rosén BG, Zahouani H, Blunt L, Mansori ME. Traceology, quantifying finishing machining and function: a tool and wear mark characterisation study. Wear 2011;271:553–8.

[12] Hafiz AMK, Bordatchev EV, Tutunea-Fatan RO. Influence of overlap between the laser beam tracks on surface quality in laser polishing of AISI H13 tool steel. J Manuf Process 2012;14:425–34.

[13] Zahouani H, Mezghani S, Vargiolu R, Dursapt M. Identification of manufacturing signature by 2D wavelet decomposition. Wear 2008;264:480–5.

[14] Wieland M, Hänggi P, Hotz W, Textor M, Keller BA, Spencer ND. Wavelength-dependent measurement and evaluation of surface topographies: application of a new concept of window roughness and surface transfer function. Wear 2000;237:231–52.

[15] Bigerelle M, Marteau J, Paulin C. Brightness versus roughness: a multiscale approach. Surf Topogr: Metrol Prop 2015;3:015004.

[16] Standardization IOf. ISO standard TS 16610-31. International organization for standardization; 2010.

[17] Daubechies I. The wavelet transform, time-frequency localization and signal analysis. IEEE Trans Inf Theory 1990;36:961–1005.

[18] Le Goic G, Favrelière H, Samper S, Formosa F. Multi scale modal decomposition of primary form, waviness and roughness of surfaces. Scanning 2011;33:332–41.

[19] Stout KJ, Matthia T, Sullivan PJ, Dong WP, Mainsah E, Luo N. et al. The developments of methods for the characterisation of roughness in three dimensions. Report EUR 15178 EN; 1993.

[20] Beucher S, Lantuejoul C. Use of watersheds in contour detection. In: Proceedings of the international work-shop on image processing, real-time edge and motion detection/estimation. Rennes; 1979.

[21] Bigerelle M, Giljean S, Mathia TG. Multiscale characteristic lengths of abraded surfaces: three stages of the grit-size effect. Tribol Int 2011;44:63–80.

[22] Persson BNJ. On the fractal dimension of rough surfaces. Tribol Lett 2014;54:99–106.

[23] Marteau J, Bigerelle M, Mazeran PE, Bouvier S. Relation between roughness and processing conditions of AISI 316L stainless steel treated by ultrasonic shot peening. Tribol Int 2015;82:319–29.

[24] Giljean S, Najjar D, Bigerelle BM, Iost A. Multiscale analysis of abrasion damage on stainless steel. Surf Eng 2008;24:8–17.

[25] Brown CA, Savary G. Describing ground surface texture using contact profilometry and fractal analysis. Wear 1991;141:211–26.

[26] Bigerelle M, Iost A. A new method to calculate the fractal dimension of surfaces: application to human cell proliferation. Comput Math Appl 2001;42:241–53.